PNAS BRIEF REPORT | APPLIED PHYSICAL SCIENCES OPEN ACCESS

Controllable synthesis of borophene aerogels by utilizing h-BN layers for high-performance next-generation batteries

Niyazi Okan Çiftçi[a,b], Sevil Berrak Şentürk[a], Yaren Sezen[a], Süreyya Üstün Kaykusuz[a], Hu Long[b], and Onur Ergen[a,b,c,1]

Edited by Alexis Bell, University of California, Berkeley, CA; received May 26, 2023; accepted August 24, 2023

Borophene is emerging as a promising electrode material for Li, Na, Mg, and Ca ion batteries due to its anisotropic Dirac properties, high charge capacity, and low energy barrier for ion diffusion. However, practical synthesis of active and stable borophene remains challenging in producing electrochemical devices. Here, we introduce a method for borophene aerogels (BoAs), utilizing hexagonal boron nitride aerogels. Borophene grows between h-BN layers utilizing boron–boron bridges, as a nucleation site, where borophene forms monolayers mixed with sp^2-sp^3 hybridization. This versatile method produces stable BoAs and is compatible with various battery chemistries. With these BoAs, we accomplish an important milestone to successfully fabricate high-performance next-generation batteries, including Na-ion (478 mAh g^{-1}, at 0.5C, >300 cycles), Mg-ion (297 mAh g^{-1}, at 0.5C, >300 cycles), and Ca-ion (332 mAh g^{-1}, at 0.5C, >400 cycles), and Li-S batteries, with one of the highest capacities to date (1,559 mAh g^{-1}, at 0.3C, >1,000 cycles).

borophene | aerogels | sodium | sulfur | next-generation batteries

Due to its distinct electrical and mechanical characteristics, emerging 2D-layered material borophene is a promising electrode material for Li, Na, Mg, and Ca ion batteries (1, 2). However, the majority of borophene polymorphs are produced at high temperatures on noble metal substrates, leading to tiny domains of mixed polymorphs, effecting stability in energy storage applications. Borophene is unstable, as it oxidizes quickly when exposed to air or moisture (3–5). Despite efforts to create borophene-based electrochemical devices, low-temperature liquid exfoliation manufactured only a few-layer 12-borophene, leading to low-yield CNT/borophene enhanced Li-S batteries (5).

We present a technique to generate stable borophene aerogel (BoA) for high-performance Li, Na, Mg, and Ca ion batteries. BoA structures are developed using a conversion method, utilizing hexagonal boron nitride aerogels (hBNAGs) as a template. To obtain a nucleation site for boron, nitrogen defects (N-defect) were chemically induced to hBNAGs, then converted to boron–boron (B-B) bridges under high-pressure boron vapor. The process is versatile and effective in producing high-performance electrodes for beyond lithium-ion batteries, utilizing borophene/h-BN hybrid aerogels (BoBN). Consequently, we enabled high-performance next-generation batteries with ultra-high performance with excellent cycling stability, retaining capacity (RC), and coulombic efficiencies (CE): Na-ion (478 mAh g^{-1}, at 0.5C, >300 cycles, RC:83%, CE:96%), Mg-ion (297 mAh g^{-1}, at 0.5C, >300 cycles, RC:87%, CE:94%), Ca-ion (332 mAh g^{-1}, at 0.5C, >400 cycles, RC:84.2%, CE:96.5%), and Li-S batteries with a remarkable capacity of 1,559 mAh g^{-1} (at 0.3C, >1,000 cycles, RC:81%, CE:95.5%). Our approach presents an effective strategy for producing stable BoBN, with exceptional properties for generating high-performance electrodes for challenging battery chemistries.

Results and Discussion

The borophene aerogels fabrication process is illustrated in Fig. 1*A*. Prepared similarly to our previous methods, BoAs were synthesized from precursors of hBNAGs (6). hBNAG was immersed into potassium hydroxide and urea propanol solution (1:1, v:v) at 60 °C. The precursors were vacuum dried, at room temperature, followed by an annealing step at 600 °C for 24 h under an Ar environment to form N-defects (Fig. 1*B*). For surface functionalization, the N-defect hBNAG was submerged into boric acid solution and vacuum dried at 80 °C. This sample was transferred to an induction furnace with boron source (Sigma-Aldrich 99.7% crystalline) and annealed at 1,400 °C for 4h, in an argon atmosphere, to form BoBN. Borophene only grew on N-defected hBNAG samples, indicating N-defects create B-B bridges, as a nucleation site for borophene (Fig. 1*C*) (7, 8). Thus, borophene can grow between two h-BN sheets, in a self-limiting manner, and form borophene/h-BN monolayers mixed with sp^2-sp^3 hybridization (Fig. 1 *D* and *E*). We believe that the volume expansion (Fig. 1*A*) is correlated with nucleation growth, but the mechanism is puzzling. Fig. 1*F* illustrates XPS analysis of BoBN samples. The B-1s spectrum reveals B-N (190.45 eV) and minor B-O

Author affiliations: [a]Department of Electronics and Communication Engineering, Istanbul Technical University, Istanbul 34469, Turkey; [b]Next-Ion-Energy Inc., Yuba City, CA 95991; and [c]Department of Mechanical Engineering, Huazhong University of Science and Technology, Wuhan 430074, China

Author contributions: N.O.Ç., S.B.Ş., Y.S., S.Ü.K., H.L., and O.E. collaborated on research, contributed tools, analyzed data, and co-authored the paper.

The authors declare no competing interest.

Copyright © 2023 the Author(s). Published by PNAS. This open access article is distributed under Creative Commons Attribution-NonCommercial-NoDerivatives License 4.0 (CC BY-NC-ND).

[1]To whom correspondence may be addressed. Email: oergen@itu.edu.tr.

Published October 9, 2023.

Downloaded from https://www.pnas.org by 78.184.195.116 on June 15, 2026 from IP address 78.184.195.116.

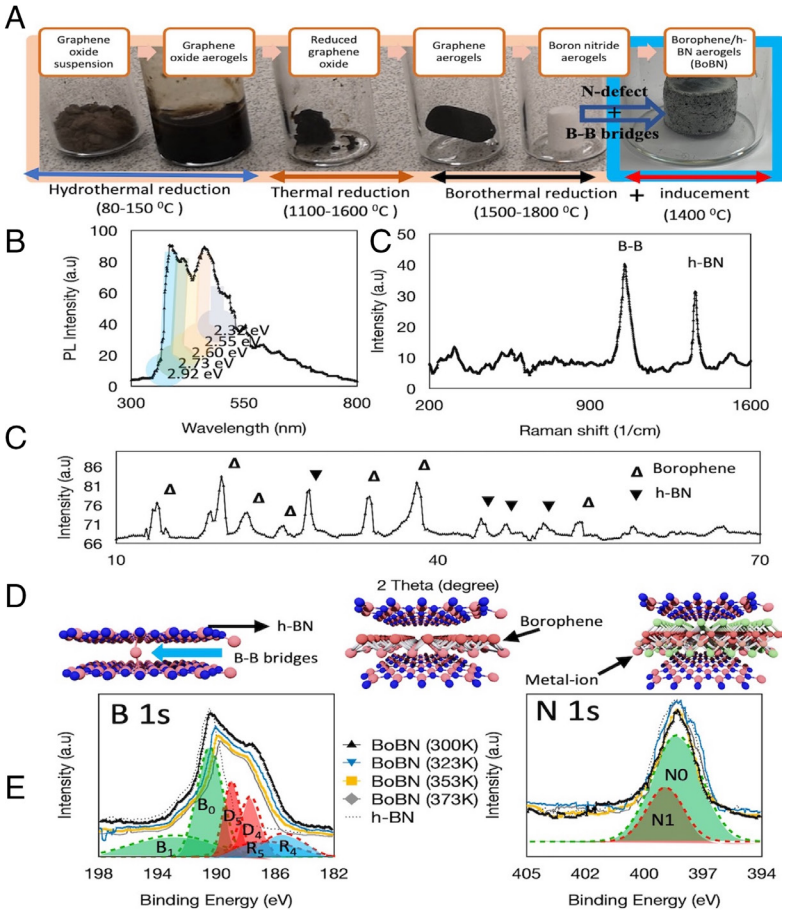


Fig. 1. (*A*) Sequential BoBN fabrication, (*B*) N-deficient h-BN PL properties, (*C*) Raman spectroscopy, (*D*) XRD patterns, (*E*) Borophene nucleation and metal-ion intercalation schematics. (*F*) XPS Analysis of BoBN's B 1s and N 1s. Coexisting B-N, B-O (B0 & B1), rectangular (R5 & R4), and diamond (D5 & D4) B-B bonds in BoBN. Oxygen annealing's B-O to B-B ratios validate robust B-B bonds and h-BN shielding.

(192.85 eV) bonds. The N 1s spectrum shows N–B (398.05 eV) and N–H (398.35 eV) bonds. The B 1s spectrum exposes intricate B-B interactions with peaks at 188.85, 185.45, 187.7, and 186.7 eV, signifying possible coexisting β_{12} and X_3 structures per literature (ID_5:ID_4 ≈ 1 and IR_5:IR_4 ≈ 1 ratios) (9, 10). However, we also acknowledge the absence of a strong sixfold (R_6) coordination, which could potentially correlate with a different phase, a plausible intermixed phase, currently presents a challenge (11). Thermal annealing in oxygen at 323 K, 353 K, and 373 K confirms durable B-B bonds, evident from consistent B-O to B-B peak ratio ~0.26 (9–11).

BoBN was used for electrode development, adapting generic fabrication techniques for producing high-performance batteries; i) Na-ion (CR2032: BoBN+10wt% CB/$NaClO_4$+ethylene/PC/Na-foil, GF separator), ii) Mg-ion (3-electrode cell: $MgMn_2O_4$ (calcination)+BoBN(1:2wt%)+10wt% CB+10wt% PVDF/graphite/Ag/AgCl in $Mg(TFSI)_2$ in THF), iii) Ca-ion (3-electrode cell: CaV_2O_5 (solid-state reaction)+BoBN, 10wt% CB+10wt% PVDF/graphite/Ag/AgCl in perchlorate), iv) Li-S (CR2032: BoBN+sulfur powder+10wt% CB+10wt% PVDF in NMP/LiPF6+EC+DMC, Celgard 2320).

The enhanced anodic stability and reversible capacity of BoBN-based batteries with different borophene/h-BN ratios, as exemplified by BoBN(5:1), BoBN(5:2), and BoBN(5:3), are shown in the galvanostatic charge/discharge curves (Fig. 2 *A–D*). BoBN-modified cells outperform control cells in long-term cycling performance (Fig. 2 *E–H*). Fig. 2*E* shows cycling performance of Na-ion batteries with and without BoBN. BoBN(5:1) shows an excellent cyclability over 300 with initial discharge (478 mAh g^{-1} at 0.5C) and good CE (>96%), while BoBN(5:2), BoBN(5:3), and samples without BoBN(W/O BoBN) exhibit 325 mAh g^{-1}, 303 mAh g^{-1}, and 137 mAh g^{-1} respectively. Evidently, cells with BoBN exhibit best performance, attributed to an increase in active sites for sodium ions, due to 3D framework and interstitial space, while lowering diffusion distances and accommodating volume changes during sodiation/desodiation processes. However, only BoBN(5:1) provided over 300 cycles, indicating that optimum loading configuration is critical to sustain efficiency of the charge and discharge process. Similarly, Fig. 2*F* indicates how important BoBN is for Mg-ion batteries anticipating a similar role as with Na-ion batteries. BoBN(5:1) shows good cyclability over 300 with initial discharge (297 mAh g^{-1} at 0.5C) and good CE (>94%), while BoBN(5:2), BoBN(5:3), and samples W/O BoBN exhibit 201 mAh g^{-1}, 152 mAh g^{-1}, and 140 mAh g^{-1} with significantly less RC but same cyclability, respectively. For Ca-ion batteries (Fig. 2*G*), only difference is that BoBN(5:3) exhibits the best performance (332 mAh g^{-1} at 0.5C) and good CE (>96.5%), while BoBN(5:1), BoBN(5:2), and samples W/O BoBN exhibit 270 mAh g^{-1}, 264 mAh g^{-1}, and 189 mAh g^{-1} with cyclability over 400, respectively. Samples W/O BoBN exhibit capacity fade and lose ability to store and release charge efficiently over 50 cycles, likely correlated with BoBN's ability to stabilize the electrolyte and prevent SEI formation. Last, Fig. 2*H* provides evidence for the importance of BoBN in preserving long-term cycling performance of Li-S batteries. At 0.3C, an initial discharge is shown of 1,559 mAh g^{-1}, 1,393 mAh g^{-1}, 1,045 mAh g^{-1}, and 810 mAh g^{-1} for BoBN(5:2), BoBN(5:1), BoBN(5:3), and commercial sulfur electrodes (CSE). All BoBN-modified batteries reached 1,000 cycles with good retention while CSE exhibited drastic capacity fade especially around 600 cycles. We speculate because of BoBN's ability to immobilize sulfur ions and highly conductive pathway. Specifically, cells with BoBN(5:2) and 4 mg/cm^2 sulfur areal mass loading exhibit best performance with better ionic diffusion and ohmic resistance, as predicted. BoBN-modified batteries show high reversible capacities at >5 C rates due to their high surface area and conductivity (Fig. 2 *I–L*), with capacities of 316, 168, 158, 1,156 mAh g^{-1} (5C) and 273, 101, 87,

Downloaded from https://www.pnas.org by 78.184.195.116 on June 15, 2026 from IP address 78.184.195.116.

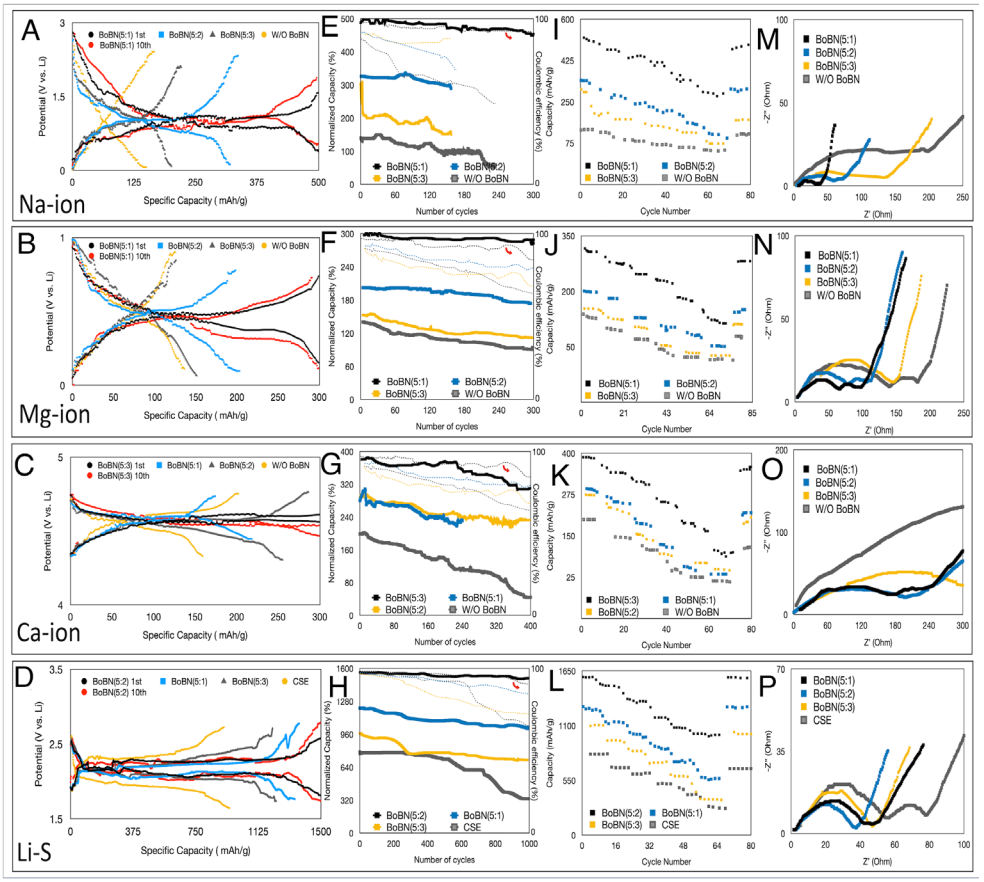


Fig. 2. Analysis of the electrochemical performance of batteries based on BoBN. The discharge–charge profiles of Na-ion (0.5C), Mg-ion (0.5C), Ca-ion (0.5C), and Li-S (0.3C) batteries, with 1st and 10th cycle, are displayed in panels (*A–D*). Long-term cyclability with CE (dashed lines) (*E–H*) and rate capabilities at 0.1C, 0.3C, 0.5C, 1C, 5C, and 10C (*I–L*). Impedance spectra for Na-ion, Mg-ion, Ca-ion, and Li-S batteries (*M–P*).

901 mAh g^{-1} (10C) for Na-ion, Mg-ion, Ca-ion, and Li-S batteries, respectively.

Several noteworthy findings must be highlighted. Na-ion, Mg-ion, Ca-ion, and multivalent ion batteries exhibit unstable behavior with nonstable overshoot capacity, at low discharge rates (<0.5C), attributed to unstable SEI on the electrode surface and limited ion transport. Additionally, the lowest coulombic efficiency for Li-S cells occurs at 1C rates, suggesting that parasitic processes impede total charge extraction. However, at high rates, BoBN aerogel undergoes self-adaptation/arrangement, mitigating these parasitic reactions.

The impedance spectra measurements demonstrate the importance of BoBN reinforcement on cell performances (Fig. 2 *M–P*). Cells, with BoBN modification, exhibit lower impedance and higher ionic conductivity compared to samples W/O BoBN. Also, semicircles at low frequencies can be associated with the presence of SEI film, apparent in Mg-ion and Ca-ion batteries. However, there is no significant charge transfer resistance at low frequencies, possibly indicating that SEI film is very thin or nonexistent for Na-ion and Li-S batteries. Cells with the proper BoBN ratio perform best, with improved ionic diffusion and ohmic resistance, yielding maximum values of 32%, 21%, 37%, and 25%, respectively. Optimal Li-S cell performance was achieved with high areal sulfur loadings and low E/S ratios. The best yield of 6% was obtained with an E/S ratio of 4.8 μL mg^{-1}, delivering an output of 811 mAh g^{-1} at 10C. This is a very important finding, being within the ideal E/S ratio <5 μL mg^{-1} (12).

Conclusion

In summary, we demonstrated a method to grow stable borophene aerogels utilizing hexagonal boron nitride, as a template. These 3D aerogels, which successfully integrated into next-generation battery chemistries, enhance ionic transport, shorten diffusion routes, and respond to volume fluctuations, enhancing stability. These innovations help us to provide one of the best-performing devices in the literature. We believe that these preliminary findings are key to unlocking many breakthroughs in energy conversion devices to achieve superior batteries in the future.

Data, Materials, and Software Availability. All study data are included in the main text.

ACKNOWLEDGMENTS. O.E. acknowledges European-Research-Council (QUEEN: 01043219) and Zettl's Lab/UC-Berkeley.

1. Z. A. Piazza *et al.*, Planar hexagonal B36 as a potential basis for extended single-atom layer boron sheets. *Nat. Commun.* **5**, 3113 (2014).
2. C. Hou *et al.*, Borophene-based materials for energy, sensors and information storage applications. *Nano Res. Energy* **2**, e9120051 (2023).
3. A. J. Mannix *et al.*, Synthesis of borophenes: Anisotropic, two-dimensional boron polymorphs. *Science* **350**, 1513–1516 (2015).
4. X. Liu *et al.*, Borophene synthesis beyond the single-atomic-layer limit. *Nat. Materials* **21**, 35–40 (2021).
5. H. Lin *et al.*, Scalable production of freestanding few-layer β12-borophene single crystalline sheets as efficient electrocatalysts for lithium-sulfur batteries. *ACS Nano* **15**, 17327–17336 (2021).
6. O. Ergen, A. K. Zettl, "High temperature Li-ion battery cells utilizing boron nitride aerogels and boron nitride nanotubes." Patent No. 10,686,227 (Lawrence Berkeley National Lab, Berkeley, CA, 2020).
7. J. M. Li, Robust 2D room-temperature dilute ferrimagnetism enhancement in freestanding ammoniated atom-thin [0001] h-BN nanoplates. *ACS Appl. Mater Interfaces* **9**, 39626–39634 (2017).
8. S. N. Grinyaev, F. V. Konusov, V. V. Lopatin, L. N. Shiyan, Optical absorption of hexagonal boron nitride involving nitrogen vacancies and their complexes. *Phys. Solid State* **46**, 435–441 (2004).
9. G. P. Campbell *et al.*, Resolving the chemically discrete structure of synthetic borophene polymorphs. *Nano Lett.* **18**, 2816–2821 (2018).
10. M. G. Cuxart *et al.*, Borophenes made easy. *Sci. Adv.* **7**, eabk1490 (2021).
11. M. Bhavyashree, S. R. Rondiya, K. Hareesh, Exploring the emerging applications of the advanced 2-dimensional material borophene with its unique properties. *RSC Adv.* **12**, 12166–12192 (2022).
12. A. Bhargav, J. He, A. Gupta, A. Manthiram, Lithium-sulfur batteries: Attaining the critical metrics. *Joule* **4**, 285–291 (2020).

Downloaded from https://www.pnas.org by 78.184.195.116 on June 15, 2026 from IP address 78.184.195.116.